Theor Chem Acc (2006) 116: 18–30
DOI 10.1007/s00214-005-0017-9

REGULAR ARTICLE

Jeremy Schofield

Quantum effects in ab-initio calculations of rate constants for chemical reactions occuring in the condensed phase

Received: 24 March 2005 / Accepted: 30 August 2005 / Published online: 4 November 2005

Abstract An overview of recent advances in the development of methods designed to calculate rate constants for chemical reactions obeying mass action kinetic equations in condensed phases is presented. A general framework addressing mixed quantum-classical systems is elaborated that enables quantum features such as tunneling effects, zero-point vibrations, dynamic quantum coherence, and non-adiabatic effects to be calculated. An efficient Monte Carlo sampling method for performing ab-initio calculations of rate constants and isotope effects in chemical processes in condensed phases is outlined, and the connection of isotope effects to reaction mechanism is explored.

1 Introduction

1.1 Phenomenology

In many situations of physical interest the dynamics of chemical systems is well-described in terms of simple differential equations that specify how coarse-grained quantities such as the mean concentrations of chemical species evolve in time. For example, in a general reaction scheme among n chemical species X_i of the form

$$\nu_1 X_1 + \cdots + \nu_n X_n \underset{k_r}{\overset{k_f}{\rightleftharpoons}} \bar{\nu}_1 X_1 + \cdots + \bar{\nu}_n X_n, \tag{1}$$

where ν_i and $\bar{\nu}_i$ are stoichiometric coefficients for the reactant and product specie i, respectively. Such a system of equations is characterized by forward and reverse rate constants k_f and k_r that appear in the mass action rate law for the average numbers (or concentrations) of a chemical species $\bar{N}_i(t)$,

$$\begin{aligned}\frac{\mathrm{d}\bar{N}_i(t)}{\mathrm{d}t} &= (\nu_i - \bar{\nu}_i)\left[-k_f \prod_{j=1}^{n} \bar{N}_j^{\nu_j}(t) + k_r \prod_{j=1}^{n} \bar{N}_j^{\bar{\nu}_j}(t)\right] \\ &= (\nu_i - \bar{\nu}_i)\, J,\end{aligned} \tag{2}$$

where J is known as the *reaction rate* [1]. Equation (2) can be used to define a progress variable $\chi(t)$ which monitors the extent of reaction

$$J = \frac{\mathrm{d}\chi(t)}{\mathrm{d}t} = (\nu_i - \bar{\nu}_i)^{-1} \frac{\mathrm{d}\bar{N}_i(t)}{\mathrm{d}t} \tag{3}$$

that may be integrated to obtain the explicit time dependence of the progress variable and thereby the deviations of all species concentrations from their equilibrium values. For dilute systems, it is often observed that the progress variable obeys the simple rate equation

$$\frac{\mathrm{d}\chi(t)}{\mathrm{d}t} = -k\chi(t), \tag{4}$$

where the overall rate constant is given by [2]

$$k = \sum_{j=1}^{n} (\nu_j - \bar{\nu}_j)\left[k_f \prod_{i=1}^{n} \left(\bar{N}_i^{\mathrm{eq}}\right)^{\nu_i} \frac{\nu_j}{\bar{N}_j^{\mathrm{eq}}} - k_r \prod_{i=1}^{n} \left(\bar{N}_i^{\mathrm{eq}}\right)^{\bar{\nu}_i} \frac{\bar{\nu}_j}{\bar{N}_j^{\mathrm{eq}}}\right].$$

Equation (4) may be integrated to yield an equation for the time evolution of the progress variable

$$\chi(t) - \chi(0) = -\int_0^t \mathrm{d}\tau\; k\,\chi(t-\tau). \tag{5}$$

1.2 Theoretical framework for calculations of rate constants

To derive the mass action rate law and obtain a microscopic expression for the rate constant k in Eq. (4), one starts from the Heisenberg equation of motion for $\hat{\chi}$ and extracts the long time evolution proportional to the slow variables of the system using projection operator techniques [2–4]. In the simplest

J. Schofield
Chemical Physics Theory Group, Department of Chemistry, University of Toronto, Toronto, ON M5S 3H6, Canada
E-mail: jmschofi@chem.utoronto.ca

approximation, one neglects the coupling of slow reactive modes and other slow degrees of the system such as hydrodynamic modes. Such approximations are reasonable provided reaction and collective diffusion of chemical species are relatively uncorrelated. From this approach, one obtains a microscopic expression corresponding to Eq. (5) [2]

$$\frac{\mathrm{d}\chi(t)}{\mathrm{d}t} = -\int_0^t \mathrm{d}\tau\ \tilde{k}(\tau)\chi(t-\tau) \tag{6}$$

and

$$\chi(t) - \chi(0) = -\int_0^t \mathrm{d}\tau \tilde{K}(\tau)\chi(t-\tau) \tag{7}$$

with

$$\begin{aligned}\tilde{K}(\tau) &= \int_0^\tau \mathrm{d}\tau_1 \tilde{k}(\tau_1) \\ &= \int_0^\tau \mathrm{d}\tau_1 \left(\mathrm{e}^{i\hat{\mathcal{Q}}\mathcal{L}\tau_1} i\mathcal{L}\hat{\chi}, i\mathcal{L}\hat{\chi}\right)\left(\hat{\chi},\hat{\chi}\right)^{-1}. \\ &= \left(\mathrm{e}^{i\hat{\mathcal{Q}}\mathcal{L}\tau}\hat{\chi}, i\mathcal{L}\hat{\chi}\right)\left(\hat{\chi},\hat{\chi}\right)^{-1}. \end{aligned} \tag{8}$$

In Eq. (8), $i\mathcal{L}$ represents the full quantum Liouville operator and $\hat{\mathcal{Q}}$ is a projection operator [3] that projects dynamical variables onto the subspace orthogonal to the slow variables and the Kubo transformed correlation function is denoted as [5]

$$\begin{aligned} C_{AB}(t;\beta) &= \beta^{-1}\mathrm{Tr}\int_0^\beta \mathrm{d}\lambda\ \hat{A}(t)\mathrm{e}^{-\lambda\hat{H}}\hat{B}^\dagger\mathrm{e}^{\lambda\hat{H}}\hat{\rho}_\mathrm{e} \\ &= \left(\hat{A}(t),\hat{B}^\dagger\right) \end{aligned} \tag{9}$$

where $\hat{\rho}_\mathrm{e}$ is the equilibrium density matrix for a system with Hamiltonian $\hat{H}$.

Since the time dependence of $\tilde{k}(\tau_1)$ arises through the projected Liouville operator $i\hat{\mathcal{Q}}\mathcal{L}$ which is orthogonal to all slow variables of the system, one expects $\tilde{k}(\tau)$ to vanish on short timescales provided there is a clear separation between microscopic times $t \sim t_\mathrm{mic}$ and the long times characterizing reactive events (and other slow motion) t_r. One therefore expects $\tilde{K}(\tau)$ to reach some constant value at an intermediate time τ^* with $t_\mathrm{mic} \ll \tau^* \ll t_r$. Since the progress variable evolves on the slow reactive time scale t_r, one sees that Eq. (6) can be written as

$$\frac{\mathrm{d}\chi(t)}{\mathrm{d}t} = -\left(\int_0^{\tau^*}\mathrm{d}\tau\tilde{k}(\tau)\right)\chi(t) + O(t_m/t_r), \tag{10}$$

thereby yielding an expression for the overall rate constant $k \approx \tilde{K}(\tau^*)$.

Unfortunately, direct calculation of $\tilde{K}(\tau^*)$ is problematic due to the projection of the dynamics orthogonal to the slow modes of the system, i.e. the presence of the projection operator $\hat{\mathcal{Q}}$ in Eq. (8). In practice, one can analyze the effect of the projection operator on the dynamics and show that, in the case in which there is a clear separation of time scale between reactive and other slow modes and the microscopic motions of the system, in fact at intermediate time scales $t \sim \tau^*$, the difference between $\tilde{K}(t)$ and the corresponding quantity calculated using the unprojected dynamics,

$$K(t) = \left(\hat{\chi}(t), i\mathcal{L}\hat{\chi}\right)\left(\hat{\chi},\hat{\chi}\right)^{-1}, \tag{11}$$

is neglible [2,6] even though the long time dynamics of $\tilde{K}(t)$ and $K(t)$ are quite different. This result was also obtained by Yamamoto [7]. Thus the calculation of the rate constant entails performing the full quantum evolution of a suitably-defined progress variable $\hat{\chi}(t)$ up to the intermediate time scale τ^* and calculating the correlation function $K(\tau^*)$ given in Eq. (11). Typically, one monitors the value of $K(t)$ until one sees a "plateau" or steady value indicating that the appropriate time scale has been reached. If no steady value is observed, it is likely that no clear separation of time scale between reactive events and the microscopic motion exists, and mass action kinetics is not likely to be an accurate description of the chemical kinetics.

2 Mixed quantum – classical systems

As is clear from the previous section, explicit calculation of the rate constant for a chemical process involves calculating the quantum evolution of operators such as $\hat{\chi}(t)$ up to intermediate time scales so that the corresponding Kubo transformed equilibrium correlation function in Eq. (11) may be evaluated. This task is effectively impossible with the current computational technology for all but the simplest systems. For many complex chemical systems, one might hope that the quantum nature of the system is relatively unimportant at high temperatures and for heavy degrees of freedom so that the classical limit of Eq. (11) may be utilized. Unfortunately, in many problems of chemical interest, quantum effects do play an important role and make a significant contribution to the reactive process, quantitatively if not also qualitatively. Nonetheless, it is frequently true that the quantum behavior of the majority of the system is unimportant, suggesting the simplification of dividing the total system into interacting quantum and classical components.

A number of procedures have been proposed [8–35] for performing molecular dynamics simulations of mixed quantum-classical systems in which quantum transitions are coupled to classical evolution. The coupling between quantum and classical subsystems is particularly important in many chemical systems containing hydrogen atoms where the nuclear motion evolves on multiple energy surfaces. In this review we focus on the approach in which the evolution of the mixed quantum-classical system is described by a quantum-classical Liouville equation [8,20,37–42]. In such a method one first takes the proper quantum-classical limit of the quantum correlation function in Eq. (11). Such a procedure [35] can be carried out by perturbatively expanding the full quantum Liouville or Heisenberg equations of motion in a small parameter characterizing the mass ratio of light (quantum) and heavy (classical) degrees of freedom [8].

Consider a general quantum system consisting of n quantum particles of mass m and N particles of mass M with a

Hamiltonian of the form

$$\hat{H} = \frac{\hat{P}^2}{2M} + \frac{\hat{p}^2}{2m} + \hat{V}(\hat{q}, \hat{Q}), \tag{12}$$

where $\hat{P}$, $\hat{p}$, $\hat{Q}$, and $\hat{q}$ are vectors of momentum and position operators of the classical and quantum degrees of freedom. The total potential energy $\hat{V}$ may be written as $\hat{V}_{\rm q}(\hat{q}) + \hat{V}_{\rm cl}(\hat{Q}) + \hat{V}_{\rm c}(\hat{Q}, \hat{q})$, where the subscripts refer to the quantum, classical and coupling terms in the potential energy. The evolution of any dynamical observable $\hat{B}$ is given by the Heisenberg equation,

$$\frac{{\rm d}\hat{B}}{{\rm d}t} = \frac{i}{\hbar}[\hat{H}, \hat{B}]. \tag{13}$$

In order to focus on the limit in which the particles with mass M, with $M >> m$, are treated classically, it is convenient to perform a partial Wigner transform with respect to the classical degree of freedom $\hat{Q}$ defined as:

$$\hat{B}_w(\mathbf{X}) = \frac{1}{(2\pi\hbar)^{3N/2}} \int {\rm d}z {\rm e}^{iP\cdot z/\hbar} \left\langle R - z/2 \middle| \hat{B} \middle| R + z/2 \right\rangle,$$

where $\mathbf{X} = (\mathbf{R}, \mathbf{P})$ and $\mathbf{R}$ is the coordinate representation of the operator $\hat{Q}$. Note that $\hat{B}_w(\mathbf{X})$ is still an operator in the quantum subspace. In the limit in which the masses of the bath (classical) particles are much larger than the quantum particle masses, a small parameter $\epsilon = (m/M)^{1/2}$ may be defined and used to perturbatively order terms [8] in the equations of motion for a partially Wigner transformed dynamical observable $\hat{B}_w(\mathbf{X})$. If terms up to first order in ϵ are retained in the full equation of motion, a Liouville equation for the mixed quantum-classical system is obtained [8]:

$$\begin{aligned} \frac{{\rm d}\hat{B}_w(\mathbf{X}, t)}{{\rm d}t} &= \frac{i}{\hbar}[\hat{H}_w, \hat{B}(t)] \\ &\quad -\frac{1}{2}\left(\left\{\hat{H}_w, \hat{B}_w(t)\right\} - \left\{\hat{B}_w(t), \hat{H}_w\right\}\right) \\ &= i\mathcal{L}\hat{B}_w(t), \end{aligned} \tag{14}$$

where the Poisson bracket notation in Eq. (14) signifies

$$\left\{\hat{H}_w, \hat{B}_w\right\} = \frac{\partial \hat{H}_w}{\partial R} \cdot \frac{\partial \hat{B}_w}{\partial P} - \frac{\partial \hat{H}_w}{\partial P} \cdot \frac{\partial \hat{B}_w}{\partial R}, \tag{15}$$

and the partial Wigner transform of the Hamiltonian is

$$\hat{H}_w(\mathbf{X}) = \frac{P^2}{2M} + \frac{\hat{p}^2}{2m} + \hat{V}_w(R, \hat{q}) = \frac{P^2}{2M} + \hat{h}_w(\mathbf{X}). \tag{16}$$

Equation (14) is solved by representing the quantum operators of the subsystem in a complete basis set. One common, and convenient, choice of basis set is the set of "adiabatic" states $|\alpha(\mathbf{R})\rangle$ which diagonalize the operator $\hat{h}_w$ defined in Eq. (16):

$$\hat{h}_w(\mathbf{R})\ |\alpha(\mathbf{R})\rangle = E_\alpha(\mathbf{R})|\alpha(\mathbf{R})\rangle\,. \tag{17}$$

Note that due to the parametric dependence of the operator $\hat{h}_w$ on $\mathbf{R}$, the basis set is R dependent. Taking matrix elements of Eq. (14), one obtains [8] the equ ation of motion for the matrix element $B_w^{\alpha\beta}(t)$

$$\frac{{\rm d}B_w^{\alpha\beta}(t)}{{\rm d}t} = i\mathcal{L}_{\alpha\beta,\alpha'\beta'}B_w^{\alpha'\beta'}(t), \tag{18}$$

where is Liouville superoperator $i\mathcal{L}_{\alpha\beta,\alpha'\beta'}$ is given by

$$\begin{aligned} i\mathcal{L}_{\alpha\beta,\alpha'\beta'} &= i\omega_{\alpha\beta}\delta_{\alpha\alpha'}\delta_{\beta\beta'} + \frac{\mathbf{P}}{M}\cdot\frac{\partial}{\partial\mathbf{R}}\delta_{\alpha\alpha'}\delta_{\beta\beta'} \\ &\quad + \frac{\mathbf{P}}{M}\cdot\left(\mathbf{d}_{\alpha\alpha'}\delta_{\beta\beta'} - \mathbf{d}_{\beta'\beta}\delta_{\alpha\alpha'}\right) \\ &\quad + \frac{1}{2}\left(\mathbf{F}_w^{\alpha\alpha'}\delta_{\beta\beta'} + \mathbf{F}_w^{\beta'\beta}\delta_{\alpha\alpha'}\right)\cdot\frac{\partial}{\partial\mathbf{P}}, \end{aligned} \tag{19}$$

with $\omega(\mathbf{R}) = (E_\alpha(R) - E_\beta)/\hbar$. In Eq. (19), quantum state couplings arise through the off-diagonal matrix terms of the non-adiabatic coupling matrix $\mathbf{d}_{\alpha\alpha'}$ given by

$$\mathbf{d}_{\alpha\alpha'} = \left\langle \alpha(\mathbf{R}) \middle| \frac{\partial}{\partial\mathbf{R}} \middle| \alpha'(\mathbf{R}) \right\rangle, \tag{20}$$

and the off-diagonal "force"

$$\mathbf{F}_w^{\alpha\alpha'} = -\left\langle \alpha(\mathbf{R}) \middle| \frac{\partial \hat{H}_w}{\partial\mathbf{R}} \middle| \alpha'(\mathbf{R}) \right\rangle. \tag{21}$$

The diagonal elements of the force matrix are the Hellmann–Feynman forces

$$\mathbf{F}_w^{\alpha\alpha} = -\frac{\partial E_\alpha(\mathbf{R})}{\partial\mathbf{R}}, \tag{22}$$

and the off-diagonal elements can be expressed [8] in terms of the non-adiabatic coupling matrix $\mathbf{d}$. Equation (18) can be conveniently written using supermatix notation in which all matrix elements $B_w^{\alpha\beta}$ are represented in a single supervector B_w^μ, with μ representing the pair (α, β) as

$$\frac{{\rm d}B_w^\mu(t)}{{\rm d}t} = i\mathcal{L}_{\mu,\nu}B_w^\nu(t), \tag{23}$$

and formally solved to obtain

$$B_w^\mu(t) = \left({\rm e}^{i\mathcal{L}t}\right)_{\mu\nu} B_w^\nu(0). \tag{24}$$

Equation (24) can be used as a starting point for exact solutions of the mixed quantum-classical equations of motion in the adiabatic basis. For systems which retain characteristics of the adiabatic ground state dynamics and involve only a small number of adiabatic energy surfaces and forces, the matrix equation can be truncated to include only a few states. For such weakly non-adiabatic systems, the matrix indices μ run over a small set of indices, resulting in a tractable system of equations.

Now returning our attention to the expression for the rate constant in Eq. (11), we see that one must evaluate the quantum-classical limit of the Kubo transformed correlation function involving the progress variable $\hat{\chi}$ and its time derivative. Recently, Sergi and Kapral [43] analyzed the quantum-classical limit of arbitrary quantum correlation functions and demonstrated that in this limit the general Kubo transformed correlation function in Eq. (9) reduces to

$$\begin{aligned} C_{AB}(t;\beta) = \sum_{\mu,\nu}\int {\rm d}\mathbf{X}_1{\rm d}\mathbf{X}_2\ B_W^{\dagger\mu}(\mathbf{X}_1, t/2)\ A_W^\nu(\mathbf{X}_2, -t/2) \\ \times W^{\mu\nu}(\mathbf{X}_1, \mathbf{X}_2; \beta), \end{aligned}$$

where $\mathbf{X}_1$ and $\mathbf{X}_2$ are the classical phase space coordinates of the bath, and $W^{\mu\nu}$ is a "spectral density function". In the high temperature, classical bath limit, one finds that the diagonal elements of the spectral density are essentially the canonical probability density with the appropriate energy, and, more generally [43],

$$W^{\alpha_1'\alpha_1;\alpha_2'\alpha_2}(\mathbf{X}_1,\mathbf{X}_2;\beta) = \frac{\mathrm{e}^{-\beta\left[P_1^2/2M+E_{\alpha_1'}(\mathbf{R}_1)\right]}}{(2\pi\hbar)^{\nu_h}\,Z_Q}\Phi^{\alpha_2\alpha_1}(\mathbf{R}_1) \times \delta_{\alpha_1',\alpha_2}\,\delta_{\alpha_2',\alpha_1}\,\delta(\mathbf{X}_1-\mathbf{X}_2), \quad (25)$$

where

$$\Phi^{\alpha_2\alpha_1}(\mathbf{R}_1) = \frac{\mathrm{e}^{\beta\left[E_{\alpha_2}(\mathbf{R}_1)-E_{\alpha_1}(\mathbf{R}_1)\right]}-1}{\beta\left[E_{\alpha_2}(\mathbf{R}_1)-E_{\alpha_1}(\mathbf{R}_1)\right]}, \quad (26)$$

ν_h is the dimension of the classical subsystem and Z_Q is the partition function

$$Z_Q = \frac{1}{(2\pi\hbar)^{\nu_h}}\sum_{\alpha}\int \mathrm{d}\mathbf{X}_1\mathrm{e}^{-\beta\left[P_1^2/2M+E_{\alpha}(\mathbf{R}_1)\right]}. \quad (27)$$

Applying this result to the rate constant, we obtain

$$k = \sum_{\mu,\nu}\int \mathrm{d}\mathbf{X}_1\mathrm{d}\mathbf{X}_2\;\chi_W^{\mu}(\mathbf{X}_1,\tau^*/2)\,\dot{\chi}_W^{\nu}(\mathbf{X}_2,-\tau^*/2) \times W^{\mu\nu}(\mathbf{X}_1,\mathbf{X}_2;\beta),$$

which reveals that the rate constant can be calculated by first drawing initial phase points $\mathbf{X}_1$ and $\mathbf{X}_2$ for the spectral density function and then propagating the partially Wigner-transformed functions χ_W and $\dot{\chi}_W$ forward and backward in time up to half the intermediate time τ^*.

2.1 Evolution schemes

2.1.1 Monte carlo sampling of non-adiabatic transitions

Although the time evolution in Eq. (24) can be evaluated by brute force diagonalization techniques for systems with few classical degrees of freedom, larger systems require somewhat more sophisticated approaches. A number of methods of tackling the numerical solution of (24) are potentially feasible. One possiblity is to separate the Liouville supermatrix operator $i\mathcal{L}$ into diagonal $i\mathcal{L}^{cl}$ and off-diagonal $i\mathcal{L}^{Q}$ components. Based on symmetries of the superoperator matrices, it can be shown that each component of the supermatrix operator has purely imaginary eigenvalues, so that the Trotter product formula

$$\mathrm{e}^{-i(\mathcal{L}^{cl}+\mathcal{L}^{Q})t} = \left(\mathrm{e}^{-\frac{i\mathcal{L}^{cl}t}{2N_t}}\mathrm{e}^{-\frac{i\mathcal{L}^{Q}t}{N_t}}\mathrm{e}^{-\frac{i\mathcal{L}^{cl}t}{2N_t}}\right)^{N_t} + O(N^{-2})$$

may be applied to approximate propagation over the total time interval as propagation over N_t short time segments of duration δt, with $t = N_t\delta t$:

$$B_w(t) = \mathrm{e}^{i\mathcal{L}^{cl}\delta t/2}M_{ad}(\delta t)\mathrm{e}^{i\mathcal{L}^{cl}\delta t/2} \cdots \mathrm{e}^{i\mathcal{L}^{cl}\delta t/2}M_{ad}(\delta t)\mathrm{e}^{i\mathcal{L}^{cl}\delta t/2}B_w(0), \quad (28)$$

with the off-diagonal matrix $M_{ad}(\delta t)$ given by

$$M_{ad}^{\mu\nu}(\delta t) = \left(\mathrm{e}^{i\mathcal{L}^{Q}\delta t}\right)_{\mu\nu}. \quad (29)$$

The "transition" matrix $\mathbf{M}_{\mu\nu}$ can be explicitly evaluated at any point in classical phase space ($\mathbf{X}$) by diagonalizing $i\mathcal{L}^{Q}$

$$\mathbf{M}_{\mu\nu}(\delta t) = \sum_{\hat{\mu}}\mathbf{S}_{\mu\hat{\mu}}(R)\mathrm{e}^{i\Omega_{\hat{\mu}}(\mathbf{R})\delta t}\mathbf{S}^{-1}_{\hat{\mu}\nu}(R), \quad (30)$$

where $|\hat{\mu}\rangle$ are the eigenvectors of $i\mathcal{L}^{Q}$, $\Omega_{\hat{\mu}}(\mathbf{R})$ are the corresponding eigenvalues, and $\mathbf{S}(R)$ is the unitary matrix which diagonalizes the $i\mathcal{L}^{Q}$ matrix written in the adiabatic basis set. Provided the system is nearly adiabatic so that the off-diagonal elements of the transition matrix are small, one can define a Monte-Carlo procedure for sampling transitions from one set of quantum labels (superindex) to another [41]. Once a transition does occur, the subsequent dynamics evolves according to the new set of quantum labels. At each moment a transition is sampled, a weight factor must be calculated to insure that the transitions are sampled properly. Thus, each trajectory has a weight factor associated with it that reflects the entire history of the sampling process. If these weights are accumulated properly, one is guaranteed that the Trotter-discretized trajectory is reproduced *exactly*. Such an approach was demonstrated in Ref. [41] on a model proton transfer system. The "transition matrix" $\mathbf{M}_{\mu\nu}$ is not a transition matrix in the proper sense in that it is not always real, positive with row sums equal to unity. This fact results in a wide distribution of weight factors and leads to numerical instabilities and slow convergence of the Monte-Carlo procedure at long times. Although these difficulties limit the applicability of the method for the calculation of the long time dynamics of the system, the method is useful for the short to intermediate time trajectories required in the calculation of rate constants.

2.1.2 Multithreads approach

Averages of dynamical variables over densities (typically probability densities) as expressed in Eq. (11) are commonly performed in analytically untractable systems by averaging a finite number trajectories starting from initial coordinates selected to represent the density. The initial coordinates are generally taken as either weighted points on a grid for low-dimensional systems or as randomly drawn points with a probability determined by the density using Monte-Carlo or other methods. In such cases, a time correlation function $\langle AB(t)\rangle$ can be approximated as

$$\begin{aligned}\langle AB(t)\rangle &= \int \mathrm{d}\mathbf{X}\;\rho(\mathbf{X})A(\mathbf{X})B(\mathbf{X}(t)) \\ &= \int \mathrm{d}\mathbf{X}\;\left[\mathrm{e}^{-i\mathcal{L}t}\left(\rho(\mathbf{X})A(\mathbf{X})\right)\right]B(\mathbf{X}) \\ &\approx \int \mathrm{d}\mathbf{X}\;\sum_{i=1}^{L}\left[\mathrm{e}^{-i\mathcal{L}t}\left(W_i\delta(\mathbf{X}-\mathbf{X}_i)\right)\right]B(\mathbf{X}), \end{aligned} \quad (31)$$

where $i\mathcal{L}$ is the classical Liouville operator, W_i is the "weight" of the initial phase point $\mathbf{X}_i = (\mathbf{R}_i, \mathbf{P}_i)$, and L is the number

of initial points sampled from the density $\rho(\mathbf{X})A(\mathbf{X})$. The statistical properties of the average are typically monitored as a function of of the initial points L which is increased until the desired level of statistical uncertainty is reached. Provided the density and the dynamical variable are smooth functions of their phase space arguments $\mathbf{R}$ and $\mathbf{P}$ at all times, L is generally found to be a relatively modest number (i.e. not prohibitivly large) even for large systems. An implicit assumption in this approach is the existence of "shadow" orbits [44] in which trajectories generated by approximate numerical methods track true trajectories. Although this shadowing property has not been proven for any complicated dynamical systems, it is generally considered to hold for real systems [45].

A similar philosophy can be applied for the mixed quantum-classical systems as well. Based on the success of applying trajectory methods to problems in classical statistical mechanics, it is interesting to consider to what extent a trajectory approach based on finite representations of phase space integrals is useful in the context of mixed quantum-classical dynamics. To pursue this line, suppose that the partial Wigner-transform of the an arbitrary operator is represented by the finite phase space matrix density

$$\hat{B}_w(\mathbf{X}) = \sum_{j=1}^{L} \mathbf{W}_j \, \delta(\mathbf{X} - \mathbf{X}_j), \tag{32}$$

where $\mathbf{W}_j$ is a matrix representing the quantum character of the operator. The matrix $\mathbf{W}$ is weighted according to the phase space arguments for each point or "thread". The utility of the discretization approach depends on the accuracy of representing any observable of physical interest by a finite and manageable number of matrices located at discrete points in classical phase space.

We now turn our attention to examining the nature of the action of the Trotter-factorized propagator on the discrete representation of an arbitrary dynamical variable expressed as in Eq. (32). The dynamics effectively consists of sequential short time propagation steps in which positions, momenta and quantum rotation of indices occurs. The Liouville (super) operator $i\hat{\mathcal{L}}$ in Eq. (19) can be written in the abstract form

$$i\hat{\mathcal{L}} = i\hat{\mathcal{L}}^Q + i\hat{\mathcal{L}}^{\mathbf{P}} + i\hat{\mathcal{L}}^{\mathbf{R}}, \tag{33}$$

where

$$i\mathcal{L}^Q B_w(\mathbf{X}) = \frac{i}{\hbar}\left[\hat{V}_w(\mathbf{R}),\, B_w(\mathbf{X})\right], \tag{34}$$

$$i\mathcal{L}^R B_w(\mathbf{X}) = \frac{\mathbf{P}}{M} \cdot \nabla_{\mathbf{R}} B_w(\mathbf{X}), \tag{35}$$

$$i\mathcal{L}^P B_w(\mathbf{X}) = \frac{1}{2}\left(\nabla_{\mathbf{P}} B_w(\mathbf{X}) \cdot \hat{\mathbf{F}} + \hat{\mathbf{F}} \cdot \nabla_{\mathbf{P}} B_w(\mathbf{X})\right), \tag{36}$$

where $\mathbf{F}(\mathbf{R}) = -\nabla_{\mathbf{R}} \hat{V}_w(\mathbf{R})$ is the "force" operator and $\hat{V}_w(\mathbf{R})$ is the partial Wigner transform of the full interation potential $\hat{V}(\hat{Q}, \hat{q})$. In Eqs. (34–36), and below, the inner product $\mathbf{A} \cdot \mathbf{B}$ denotes $\sum_{i=1}^{N} \mathbf{A}_i \cdot \mathbf{B}_i$.

First, the operator $i\mathcal{L}^Q$ does not involve derivatives with respect to the classical coordinates and therefore operates only on the quantum subspace of the dynamical variable. In super-vector notation, we therefore obtain

$$\left(\mathrm{e}^{-i\mathcal{L}^Q \delta t}\right)_{\mu\nu} \sum_{j=1}^{L} \mathbf{W}_j^{\nu} \delta(\mathbf{X} - \mathbf{X}_j) = \sum_{j=1}^{L} \mathbf{W}_j^{\mu}(\delta t) \delta(\mathbf{X} - \mathbf{X}_j), \tag{37}$$

where $\mathbf{W}_j^{\mu}(\delta t)$ is easily evaluated by transforming to and from the basis in which the superoperator $i\mathcal{L}^Q$ is diagonal. The operation of the spatial operator $\exp\{-i\mathcal{L}^R \delta t\}$ shifts the spatial location of the jth thread from position $\mathbf{R}_j$ to $\mathbf{R}_j + \mathbf{P}_j \delta t/m$. The action of the momentum propagator $i\mathcal{L}^P$ on the dynamical variable is somewhat more complicated due to the off-diagonal forces. Using the transformation matrices introduced in Eq. (30) to diagonalize the off-diagonal component of $i\mathcal{L}$, the momentum propagation step of a particular component P_k can be written as

$$\left(\mathrm{e}^{-i\mathcal{L}^{P_k} \delta t}\right)_{\mu\nu} \sum_{j=1}^{L} \mathbf{W}_j^{\nu} \delta(\mathbf{R} - \mathbf{R}_j)\delta(\mathbf{P} - \mathbf{P}_j) = \sum_{j=1}^{L} S_k^{\mu\gamma}(\mathbf{R})\, \tilde{\mathbf{W}}_j^{k,\gamma} \delta(\mathbf{R} - \mathbf{R}_j)\, \delta(\mathbf{P} - \mathbf{P}_j^{k,\gamma}(\delta t)), \tag{38}$$

where $\mathbf{P}_j^{k,\gamma}(\delta t) = (P_1, \ldots, P_{k-1}, P_k + F_k^{\gamma} \delta t, \ldots, P_N)$ and $\tilde{\mathbf{W}}^k = S_k^{-1}(\mathbf{R}) \cdot \mathbf{W}$. Again, note that, in general, each component $\tilde{W}^{\gamma}$ of the super-vector $\tilde{\mathbf{W}}$ evolves according to a different force, F^{γ}. If the effective dimension of the quantum subspace is d_q so that the super-vector $\tilde{\mathbf{W}}$ is a D-dimensional column vector, where $D = d_q * (d_q + 1)/2$, which can be decomposed as follows:

$$\tilde{\mathbf{W}} = \begin{pmatrix} w_1 \\ w_2 \\ \vdots \\ w_D \end{pmatrix} = \begin{pmatrix} w_1 \\ 0 \\ \vdots \\ 0 \end{pmatrix} + \begin{pmatrix} 0 \\ w_2 \\ \vdots \\ 0 \end{pmatrix} + \cdots + \begin{pmatrix} 0 \\ 0 \\ \vdots \\ w_D \end{pmatrix} = \tilde{\mathbf{X}}_1 + \tilde{\mathbf{X}}_2 + \cdots + \tilde{\mathbf{X}}_D. \tag{39}$$

The matrix product $S_k(\mathbf{R})\, \tilde{\mathbf{W}}^k$ in Eq. (38) implies that every thread may be written as a linear combination of D new threads with a super-vector $S_k(\mathbf{R})\tilde{\mathbf{X}}_i$, where each of the threads has different P_k arguments. From these considerations, one may interpret the consequence of the off-diagonal nature of the momentum propagator as leading to the branching of one thread into D new threads along each of the $3N$ momentum degrees of freedom. Hence, the total number of threads after a *single* momentum propagation step along a particular degree of freedom increases by a factor of D from the current number L to $D \times L$. Clearly the number of threads grows exponentially with propagation timestep and with the number of non-commuting force matrices.

One can thus summarize the propagation scheme as follows: for each time step, the spatial coordinates are updated

according to the current momenta after which the transformation supermatrices $S_k(\mathbf{R})$ are constructed and the momenta P_k are updated in sequential fashion. This is carried out by transforming the super-vector $\mathbf{W}$ for each of the threads into the appropriate force representation in which the momentum propagator of P_k is diagonal. D threads are created from each old thread out of the individual elements of $\mathbf{W}$ and the momentum argument for the phase point for each of them is propagated with the diagonal forces for that element. After propagation, all threads are transformed back into the original representation and the process is repeated. Following the propagation of all momenta, the super-vectors undergo a quantum rotation as described in Eq. (37). On the other hand, only L threads should be sufficient to describe to represent the dynamical variable accurately. Hence, from a practical point of view, since the function the threads represent is localized in finite regions of phase space and relatively smooth by assumption, many of the threads generated by the off-diagonal nature of the forces involved in the momentum propagation steps are redundant. It is therefore desirable to selectively prune the large number of new threads created by the propagation procedure to retain only those threads which are necessary to represent the dynamical variable well.

The central idea in the "multithreads" algorithm is to combine threads which approach one another in classical phase space in a manner consistent with conservation principles. The utility of the combination principle relies on the notion that if two threads approach one another in a region in which the dynamical variable is smooth, one thread is likely to be redundant so that the two adjacent threads can be combined into a single thread. In the simplest implementation of the method, all nearest thread pairs are searched for and then as many pairs of threads are combined as is necessary to keep the total number of threads at specific levels determined by issues such as the continuity of expectation values (such as populations or average trajectories) and energy conservation. Under these rules, the trajectories (threads) which are generated interact in a simple fashion, in contrast to most methods which use classical trajectories to describe quantum dynamics.

The multithreads algorithm has been applied to model proton transfer processes [41], on model two-level systems coupled to a classical coordinate [46] devised specifically to test particular quantum scattering features [47], as well as model systems [48,49] in which multiple classical degrees of freedom couple explicitly to a quantum subsystem [50]. For all models, the multithreads algorithm yields results which show excellent agreement for all quantities calculated at a relatively modest cost involving a manageable number of threads. The quality of the results obtained is insensitive to the order in which Trotter decomposition of the various components of the mixed quantum-classical Liouville operator is carried out.

In spite of these successes, a number of issues remain to be addressed concerning the general applicability of the propagation scheme. Foremost among these is to assess the range of validity of the multithreads algorithm so that some idea of what specific conditions must be met for such an approach to be fruitful. Given the uncontrolled nature in which the thread pruning occurs, it is difficult to make direct theoretical estimations of such limits. Nonetheless, either algorithm outlined here should be adequate to propagate the mixed quantum-classical systems for the short times required to provide estimates of the rate constant for chemical processes.

3 Adiabatic limit and transition state theory

In a mixed quantum-classical system, transitions among states in the quantum subsystem result from the nonadiabatic coupling matrix $\mathbf{d}$ defined in Eq. (20). In many systems, the matrix $\mathbf{d}$ is small and can be neglected. A notable exception to this simplification occurs in systems where the adiabatic energy surfaces $E_\alpha(\mathbf{R})$ are degenerate or nearly-degenerate, leading to conical intersections and avoided crossings. However even for these systems the nonadiabatic coupling matrix is neglible in most arrangements of the system, so that quantum transitions only occur when the system is in a specific configuration, typically near a so-called "transition state".

When the nonadiabatic coupling matrix is neglible and the adiabatic energy states are well separated with respect to kT, the mixed quantum-classical formalism simplifies into the adiabatic limit. In this case, the dynamics of the system in a specific quantum state is completely uncoupled from all others and the momenta evolve according to the standard Hellmann-Feynman forces for that state. Furthermore, the spectral density function given in the high temperature limit in Eq. (25) is diagonal in quantum indices and phase space argurments, and assumes the standard canonical form

$$\begin{aligned} W^{\alpha_1'\alpha_1;\alpha_2'\alpha_2}(\mathbf{X}_1,\mathbf{X}_2;\beta) &= \frac{\mathrm{e}^{-\beta\left[P_1^2/2M+E_0(\mathbf{R}_1)\right]}}{(2\pi\hbar)^{\nu_h}\, Z_Q} \\ &\quad\times\delta_{\alpha_1',\alpha_2}\,\delta_{\alpha_2',\alpha_1}\,\delta_{\alpha_1,0}\,\delta_{\alpha_2,0}\,\delta(\mathbf{X}_1-\mathbf{X}_2), \\ &= f_{\mathrm{e}}(\mathbf{X}_1) \end{aligned} \tag{40}$$

where $E_0(\mathbf{R}_1)$ is the ground adiabatic energy. Under these conditions, one may simplify the expression for the rate constant to

$$K(\tau^*) = \left\langle \dot{\chi}\,\chi(\tau^*)\right\rangle \langle \chi\,\chi\rangle^{-1}, \tag{41}$$

where $\langle\cdots\rangle$ denotes the average with respect to the canonical equilibrium probability density f_{e} with an energy given by the sum of the kinetic energy and the potential energy of the ground state adiabatic surface. In Eq. (41), the time evolution is governed by the standard classical Liouville operator with the forces given by the Helmann–Feynman forces in the ground adiabatic state $\mathbf{F}(\mathbf{R}) = -\partial E_0(\mathbf{R})/\partial\mathbf{R}$.

Within the context of the chemical kinetics developed here, it has implicitly been assumed that the phase space has at least two domains of attraction in which the system spends long periods of time with rare and rapid transitions among them. To apply the formalism outlined here, one must define a reaction coordinate $\xi(\mathbf{R})$ of low dimensionality that characterizes transitions from one basin to another. Viewed in

isolation, the dynamics of the reaction coordinate appears stochastic in which the other degrees of freedom can either donate or remove energy. In order to make an escape from one well, the stochastic variable $\xi(t)$ must acquire energy to become activated toward the barrier and, upon reaching the barrier top, it must again lose energy to become trapped in the neighboring well. If one defines the reaction coordinate so that $\xi > 0$ corresponds to one well (henceforth called a product state) and $\xi < 0$ corresponds to the other (called a reactant state), then the progress variable χ can be taken to be [2]

$$\chi(\mathbf{R}) = -\left(\theta\big(\xi(\mathbf{R})\big) - \big\langle\theta\big(\xi(\mathbf{R})\big)\big\rangle\right), \tag{42}$$

where $\theta(x)$ is the Heaviside function. Inserting this definition into the expression for the rate constant, we obtain [7]

$$K(\tau^*) = \left\langle\dot{\xi}\delta(\xi)\theta(\xi(\tau^*))\right\rangle\langle\chi\,\chi\rangle^{-1}, \tag{43}$$

which may be rewritten as[51]

$$K(\tau^*) = k_{\mathrm{TST}}\kappa(\tau^*) \tag{44}$$

with a "transition state theory" expression for the rate constant defined to be the $\tau^* = 0^+$ limit of the rate constant

$$k_{\mathrm{TST}} = \left\langle\dot{\xi}\delta(\xi)\theta(\dot{\xi})\right\rangle\langle\chi\,\chi\rangle^{-1}, \tag{45}$$

and a "transmission coefficient" given by

$$\kappa(t) = \frac{\left\langle\dot{\xi}\delta(\xi)\theta(\xi(\tau^*))\right\rangle}{\left\langle\dot{\xi}\delta(\xi)\theta(\dot{\xi})\right\rangle}. \tag{46}$$

The usefulness of the breakdown in terms of a transition state rate constant and a transmission coefficient depends on the accuracy of the assumption that the value of the rate constant is determined to a large extent by the short time behavior of $K(t)$. Examination of Eq. (43) indicates that the neglect of the transmission coefficient (known as transition state theory, abbreviated as TST) amounts to assuming that when the system, initially constrained at the top of the barrier (or in the transition state) is initially directed to the product (reactant) state, it remains in that state for all times. Thus TST allows an upper bound for the rate constant to be computed. The transmission coefficient or recrossing factor can be calculated by running dynamical trajectories that start at the top of the barrier [52]. The recrossing factor is essentially the fraction of trajectories which are stabilized after a transient relaxation in the state to which they were initially directed. For a chemical process, the TST transition rate in Eq. (45) can be written, after integration over the momenta, as

$$k_{\mathrm{TST}} = \sqrt{\frac{1}{2\pi\beta m_H}}\frac{\int \mathrm{d}\mathbf{R}\ \mathrm{e}^{-\beta E_0(\mathbf{R})}\, w(\mathbf{R})\,\delta(\xi(\mathbf{R}))}{\int \mathrm{d}\mathbf{R}\ \mathrm{e}^{-\beta E_0(\mathbf{R})}\,\theta(\xi(\mathbf{R}))}, \tag{47}$$

where the integral extends over the entire configurational space of the system, the prefactor for the fraction of averages is the thermal velocity of a hydrogen atom at temperature T, and the denominator of the ratio is the partition function of the reactant. The weighting factor $w(\mathbf{R})$ arises from the momentum integration, and is given by

$$w(\mathbf{R}) = \sqrt{\sum_i \frac{m_H}{m_i}\left(\frac{\partial\xi}{\partial\mathbf{r}_i}\right)^2} \tag{48}$$

for a one-dimensional reaction coordinate. Note that $w(\mathbf{R})$ depends on the dimensionless mass ratios m_i/m_H due to the prefactor in Eq. (47). In the case where the reaction coordinate is one of the Cartesian spatial coordinates $\mathbf{r}_i$ of the system, $w(\mathbf{R}) = 1$ and the TST transition rate may be written as

$$k_{\mathrm{TST}} = \sqrt{\frac{1}{2\pi\beta m_i}}\frac{\mathrm{e}^{-\beta\phi(0)}}{\int_0^\infty \mathrm{d}\xi\ \mathrm{e}^{-\beta\phi(\xi)}}, \tag{49}$$

where $\phi(\xi) = -kT\log\langle\delta(\xi(\mathbf{x}) - \xi)\rangle$ is the potential of mean force. Equation (49) demonstrates that the potential of mean force is intimately related to the expression for the reaction rate in the TST approximation. As is evident from Eq. (47), the calculation of TST rate requires only straightforward configurational averages in a classical system.

3.1 Correlation-reduction techniques

From a practical point of view an estimator for the fraction in Eq. (47) is given by

$$\frac{\int \mathrm{d}\mathbf{R}\mathrm{e}^{-\beta E_0(\mathbf{R})} w(\mathbf{R})\delta(\xi(\mathbf{R}))}{\int \mathrm{d}\mathbf{R}\mathrm{e}^{-\beta E_0(\mathbf{R})}\theta(\xi(\mathbf{R}))} = \hat{J} = \frac{\hat{J}_1}{\hat{J}_2}, \tag{50}$$

where

$$\hat{J}_1 = \frac{1}{\triangle\xi}\sum_{\mathbf{R}^i} w(\mathbf{R}^i)[0 \le \xi(\mathbf{R}^i) \le \triangle\xi] \tag{51}$$

$$\hat{J}_2 = \sum_{\mathbf{R}^i}[0 \le \xi(\mathbf{R}^i)], \tag{52}$$

where $\mathbf{R}_i = \{r_1^i, r_2^i, \ldots, r_N^i\}$ are the N spatial coordinates of the system for configuration i in the Markov chain constructed so that states generated are asymptotically distributed according to $P(\mathbf{R}) = \exp\{-\beta E_0(\mathbf{R})\}/Z$. In the equations above we have used Iverson's convention [53] which consists of placing a Boolean expression in square brackets and requiring that the result is 1 if the expression is *true* and 0 if it is *false*. Note that in Eq. (51), $\Delta\xi$ should be chosen to be small enough so that $\frac{1}{\Delta\xi}[0 \le \xi(\mathbf{R}^i) \le \Delta\xi]$ is a good approximation of the delta function $\delta(\xi)$, but large enough such that the variance of the estimator $\hat{J}_1$ is not too big in order to guarantee that there are enough points inside the interval.

A simulation can give only a confidence interval for the expected value of an estimator. Usually this is given in terms of 95% confidence intervals,

$$\{E[\hat{J}] - 2\sqrt{\mathrm{Var}[\hat{J}]},\ E[\hat{J}] + 2\sqrt{\mathrm{Var}[\hat{J}]}\}, \tag{53}$$

where $E[\hat{J}]$ is the estimated value from the simulation. The variance $\mathrm{Var}[\hat{J}]$ of $\hat{J}$ depends on the number of independent points, or equivalently on the the integrated correlation time. In general, if $\hat{J}$ is an estimator of a quantity obtained using the N configurations which are the output of a Markov

Chain after eliminating the burn-in length of the simulation [54], then

$$f = \frac{\sqrt{\mathrm{Var}[\hat{J}]}}{E[\hat{J}]} \sim \frac{1}{\sqrt{n_p}}, \tag{54}$$

where n_p is the number of independent points in the region of the barrier top and f is the ratio between the standard error and the estimated value. Generally speaking, the analysis of statistical uncertainties as presented here assumes that the points retained in the simulation are essentially uncorrelated and distributed normally. In fact, the distribution of values for any given observable is often not normal and hence not entirely specified by the mean and variance [55] (see Ref. [56] for an example in which the data are non-normally distributed).

The accuracy of the estimation of the classical rate constant k_{TST} obtained from the simulation therefore increases as the square root of the number of independent points in the activated region.

The calculation of the rate constant therefore amounts to generating an appropriately-distributed Markov Chain of states. However the generation of such a sequence of configurations using standard methods, either molecular dynamics (MD) or Monte Carlo methods (MC), effectively requires the calculation of the energy of the adiabatic ground state of each configuration. Given that molecular mechanics potentials are generally parameterized for stable, non-reactive configurations, the accurate estimation of such energies for chemical processes in which covalent bonds are broken and formed often neccesitates the use of computationally demanding ab initio electronic structure methods, such as density function theory (DFT). The use of such methods precludes the possibility of generating very long sequences of configurations, and it is therefore essential to consider means of maximizing the number of independent points n_p in the chain of states.

Iftimie et al. [57] proposed a method to decrease the correlation of output data using an importance function method [54]. The basic idea of importance function method consists of using an auxiliary density function $g(\mathbf{x})$ from which one can easily sample points according to their correct weight yet is similar to the target density function $f(\mathbf{x})$. In the context of Markov chain Monte Carlo simulations, this means that if the actual state of the chain is $\mathbf{x}_i$, the proposed point $\mathbf{x}_f$ drawn from the distribution $g(\mathbf{x})$ should be accepted with the probability

$$\min\left\{1, \frac{f(\mathbf{x}_f)}{g(\mathbf{x}_f)}\frac{g(\mathbf{x}_i)}{f(\mathbf{x}_i)}\right\} \tag{55}$$

to ensure that the configurations in the Markov chain are asymptotically distributed according to $f(\mathbf{x})$. When trial states $\mathbf{x}_f$ are drawn from a distribution very similar to the target distribution, nearly all the points will be accepted and the successive configurations will be essentially uncorrelated provided that the trial states $\mathbf{x}_f$ is independent of $\mathbf{x}_i$. For complicated importance functions $g(\mathbf{x})$, the simplest means of sampling new trial configurations is to utilize an auxiliary Markov chain which has limiting distribution $g(\mathbf{x})$. Provided the trial states are selected as the output of sufficiently long intervals on the auxiliary Markov chain, each proposed state for the target Markov chain is essentially independent of the current state. In an ab-initio MC simulation, drawing trial configurations from a distribution based upon a molecular mechanics potential, or any other efficient means of estimating the potential energy, using a supplementary Markov chain will increase the total cpu time by a very small factor since calculating the classical energy of a configuration is several orders of magnitude faster than the same ab-initio calculation.

In this approach, called the molecular mechanics based importance sampling method (MMBIF) [57], each trial configuration is obtained as the last state in a series of molecular mechanical based updates starting from the current configuration in the ab initio simulation. The proposed configurations are then accepted or rejected in the ab initio chain according to the usual Metropolis–Hastings algorithm [57]. If the previous and new trial configurations in the ab initio MC chain are denoted by $\mathbf{x}_{\mathrm{old}}$ and $\mathbf{x}_{\mathrm{new}}$, respectively, the proposed state is accepted with the probability $\min\{1, \exp(-\beta\triangle\triangle E)\}$, where $\triangle\triangle E$ is defined to be

$$\begin{aligned}\triangle\triangle E = &(E^{\mathrm{DFT}}(\mathbf{x}_{\mathrm{new}}) - E^{mm}(\mathbf{x}_{\mathrm{new}})) \\ &-(E^{\mathrm{DFT}}(\mathbf{x}_{\mathrm{old}}) - E^{mm}(\mathbf{x}_{\mathrm{old}})),\end{aligned} \tag{56}$$

where $E^{\mathrm{DFT}}(\mathbf{x})$ and $E^{\mathrm{cl}}(\mathbf{x})$ are the potential energies of configuration $\mathbf{x}$ calculated by ab initio methods and the molecular mechanical potential, respectively (see Fig. (1) for a schematic of the algorithm). It is straightforward to show that this acceptance criterion guarantees that the ab initio Markov chain has the correct limiting Boltzmann distribution [57], regardless of the number of auxiliary updates used to generate the proposed configuration.

The MMBIF approach has been applied to study the potential of mean force for a system composed of formic acid and water [57] as well as to study the concerted proton transfer that takes place between acetic acid and methanol in a solution of tetrahydrofuran [58]. In both studies the utilization of the molecular-mechanics-based importance function decreases the correlation time of the ab-initio MC calculation by orders of magnitude. Simulations performed without importance sampling require much more computational time to obtain comparable levels of accuracy. Furthermore,

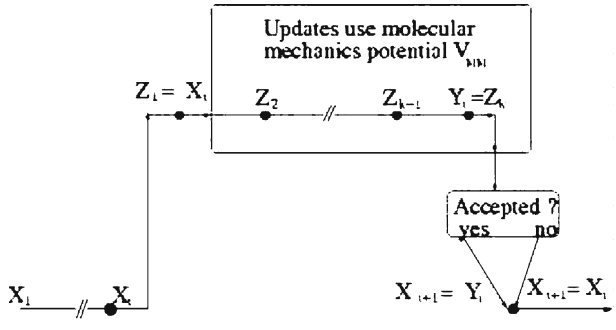

Fig. 1 Schematic of the MMBIF sampling method

the MC importance sampling method enables a thorough sampling of the relevant configurational space which allows accurate estimates of transition state theory rate constants to be obtained from relatively short simulations.

In addition, several critical performance issues of the approach, such as the efficiency of the method in the event of moderate agreement of the guiding potential and the ab initio energy, have been analyzed [57]. It has been demonstrated that separating the variables to be updated in a molecular mechanics MC step into several groups will improve the mobility of the simulation. If possible, one group should contain variables which are strongly correlated. In general, separating the variables into groups should permit efficient sampling of configurational space when the distribution of states which are poorly estimated by the guiding potential is relatively random, even for molecular mechanics potentials which overestimate or underestimate the energy by a few kT.

If long periods of MC rejections still exist, this is an indication that there is an important disagreement between the molecular mechanics and the ab-initio density of states which is very likely localized in some region of the state space. A remedy for this problem is to combine the importance sampling described above with another method, which generates a different Markov chain dynamics. For example, configurations proposed with a different molecular mechanics potential, including umbrella sampling potentials, could be used to move the simulation away from the problematic region of state space. Another means to avoid becoming trapped in phase space would be to use ab-initio Metropolis updates and the usual Metropolis criteria for acceptance. An equally good solution is to combine importance sampling with ab-initio MD when accurate calculation of the forces is possible. It has been demonstrated [57] that these two simple techniques are enough to obtain integrated times which are at most one order of magnitude bigger than in the case where a very good molecular mechanics potential is available.

4 Kinetic isotope effects and reaction mechanism

The concept of reaction mechanism plays a major role in chemistry and represents a synthesis of our understanding of the way in which different topological changes in the bonding structure of a reactant or product are correlated as the reaction proceeds. To date, most experimental investigations of complex reaction mechanisms taking place in liquid environments are still inferred from isotope and solvent (medium) effects on the reaction rate [59–61]. Consequently, the interpretation of the experimental results as well as the reaction mechanisms inferred are often controversial. Computer studies can be useful as a complement to experimental data in cases where experiments alone cannot provide a definitive picture of the mechanism of the chemical process. It is therefore desirable to develop systematic computational approaches to carefully examine the relation between isotope effects and reaction mechanism in condensed phase systems.

The study of secondary isotope effects in model reactions is also important in understanding the conditions under which mixed quantum-classical schemes can be applied to simplify the description of a complicated quantum problem. Since classical behavior is obtained for any atom whose mass is sufficiently large, computational studies of kinetic isotope effects provide a powerful means of analyzing the conditions in which an increase in the nuclear mass of an atom does not significantly alter the overall kinetics. Such a condition is a *minimal* requirement for the classical treatment of the atom. Intuitively, one might anticipate that primary atoms explicitly involved in the bond-forming and bond-breaking events should be treated within a quantum mechanical framework. However, there is less consensus on whether or not secondary atoms not *directly* involved in chemical events must be treated in a quantum mechanical fashion. Fictitious isotopic substitution can hence be used to explore the conditions in which the quantum behavior of collective motions of secondary atoms must be considered.

The path integral formalism of quantum mechanics provides a practical route for computing kinetic isotope effects via a quantum analog of transition state theory for quantum activated processes [65,66]. In this formalism, quantum particles are mapped onto closed paths $\mathbf{r}(t)$ in imaginary time t with $0 \le t \le \beta\hbar$ [63]. In practical implementations, discretizations of the closed paths leads to an isomorphism between the path integral formalism and a system of interacting ring polymers with P beads governed by the effective potential

$$E_{\text{eff}} = \sum_{i=1}^{N} \frac{P m_i (k_B T)^2}{2\hbar^2} \sum_{p=1}^{P} (\mathbf{r}_i^{(p)} - \mathbf{r}_i^{(p+1)})^2 + \frac{1}{P} \sum_{p=1}^{P} E_0(\mathbf{r}_1^{(p)} \cdots \mathbf{r}_N^{(p)}), \tag{57}$$

where N is the number of atoms, m_i the mass of atom i, and $\mathbf{r}_i^{(p)}$ is the position of bead p of atom i. In Eq. (57), the closure of the Feynman path is imposed by periodic boundary conditions $\mathbf{r}_i^{(j)} = \mathbf{r}_i^{(P+j)}$, and $E_0(\mathbf{r}_1, \ldots, \mathbf{r}_N)$ is the ground state potential energy calculated either by ab initio methods or by a molecular mechanics potential. The first term on the right-hand side of Eq. (57) describes harmonic interactions between the beads and is related to the average quantum kinetic energy. In the limit of an infinite number of beads, the discrete representation of the paths becomes exact and averages over the canonical Boltzmann distribution $\exp(-E_{\text{eff}}/kT)/Q$ yield the full quantum canonical ensemble averages. In practice, however, only approximately $P = 20$ beads are required for each nucleus to obtain converged quantum averages for many systems. The classical limit is recovered as the masses $m_i \to \infty$, in which case the polymer representing the quantum particle collapses onto the center-of-mass or *centroid* of the ring polymer

$$\overline{\mathbf{r}_i} = \frac{1}{P} \sum_{p=1}^{P} \mathbf{r}_i^{(p)}. \tag{58}$$

The path integral approach has been utilized to formulate an approximate theory of quantum activated processes using the notion that the reaction rate is governed by the activation free

energy for the centroid reaction coordinate [65,66] and that dynamical recrossing is unimportant for good choices of the reaction coordinate.

The application of the MMBIF method in the context of path-integral simulations consists of using the effective potential energies $E_{\text{eff}}^{\text{DFT}}$ and E_{eff}^{mm} calculated via ab initio and molecular mechanical potentials, where $E_{\text{eff}}^{\text{DFT}}$ and E_{eff}^{mm} represent the effective potential energy in Eq. (57) with $E(\mathbf{r}_1, \ldots, \mathbf{r}_N)$ defined by E^{DFT} and E^{mm}, respectively. Since the acceptance criterion used in the MMBIF method [see Eq. (56)] involves only the difference between the effective potential energies $\Delta\Delta E_{\text{eff}}$, it is evident the relevant energy differences for the MC procedure are independent of the kinetic energy terms, and

$$\Delta\Delta E_{\text{eff}} = \frac{1}{P}\sum_{p=1}^{P}\Delta E(\mathbf{r}_{1,\text{new}}^{(p)}\cdots\mathbf{r}_{N,\text{new}}^{(p)}) - \frac{1}{P}\sum_{p=1}^{P}\Delta E(\mathbf{r}_{1,\text{old}}^{(p)}\cdots\mathbf{r}_{N,\text{old}}^{(p)}), \tag{59}$$

where $\Delta E(\mathbf{r}_1^{(p)}\cdots\mathbf{r}_N^{(p)}) = E^{\text{DFT}}(\mathbf{r}_1^{(p)}\cdots\mathbf{r}_N^{(p)}) - E^{mm}(\mathbf{r}_1^{(p)}\cdots\mathbf{r}_N^{(p)})$. The auxiliary classical Markov chain used to propose MC updates in the MMBIF procedure allows for rapid equilibration of the discretized paths representing nuclei. As a consequence, the polymer bead conformations are essentially statistically independent in successive proposals. This is in sharp contrast to dynamical methods of sampling the effective distribution in which sophisticated staging and thermostating methods are necessary to equilibrate the paths [64]. Unfortunately the calculation of the ab initio effective potential $E_{\text{eff}}^{\text{DFT}}$ is computationally demanding, since P energy calculations must be carried out for each path conformation.

In Ref. [67], an extended version of the MMBIF sampling method was applied in the context of imaginary time path integral simulations of the tautomerization proton-transfer reaction in malonaldehyde solvated by an aprotic, nonpolar solvent (see Fig. 2).

It was demonstrated that ad hoc bond-energy bond-order relations derived from bond evolution theory [68,69] combined with Pauling's valence bond ideas [70] can be used to construct a molecular mechanics guiding potential for the ab initio simulation that improves the statistics by three orders of magnitude [67]. There are several advantages in constructing a classical potential for a reactive system in this manner. First, it provides a simple way to enforce the chemically intuitive idea that the reaction path is determined primarily by the atoms involved in the bond-breaking and bond-forming processes. This hypothesis is based on experimental evidence which suggests that primary kinetic isotope effects, which involve isotopic substitution of atoms directly involved in chemical bond breaking/forming processes, are generally orders of magnitude [71] larger than secondary kinetic isotope effects due to substitutions of other atoms. It is much more difficult to implement such a constraint in other approaches, such as the commonly-applied empirical valence bond method [72], which necessitates a special functional form for the off-diagonal coupling. Second, useful built-in empirical chemical concepts such as the partial bond order can easily lead to interpretations of the reaction mechanism.

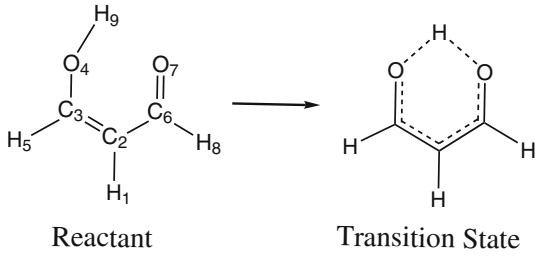

Fig. 2 The proton transfer tautomerization reaction in the enol form of malonaldehyde

In Ref. [56] and [73], two different bond evolution theory molecular (BET) mechanical potentials were constructed to study how the quality of a molecular mechanics description of the reactive energy surface influences the accuracy of predicted kinetic isotope effects. The potentials were constructed as the sum of two terms. The first term consisted of a double-well potential depending on a control parameter ξ_1 which is a function of only the coordinates of the atoms directly involved in the bond-breaking and bond-forming processes

$$\xi_1 = \frac{d_{O_4H_9} - d_{O_7H_9}}{d_{O_4O_7}}. \tag{60}$$

This term was identical in the two molecular mechanics potentials. The second term consisted of a sum of harmonic potentials taken to depend parametrically on ξ_1 The second type of potentials describe the evolution of the bond, bond angle and dihedral motions during the reaction. The difference between the two molecular mechanics potentials consisted of the functional form of the parametrical dependence of the carbonylic and enolic bond lengths on ξ_1. In the first potential, BET1, the bond lengths varied linearly with ξ_1, while for the second potential, BET2, a tangent hyperbolic variation was utilized. For these model systems, as well as the ab initio system, calculations of the indicator

$$r = \log\frac{k_{^1H,^{12}C}}{k_{^1H,^hC}} / \log\frac{k_{^3H,^{12}C}}{k_{^3H,^hC}} \tag{61}$$

were carried out [56]. The magnitude of r is often used in the physical organic chemistry literature as a measure of the extent to which secondary atoms are involved in tunneling. The value $r = 1$ corresponds to the *rule of geometric mean*, which has been empirically found to be valid [74–78] when reaction rates are calculated using a simple semi-classical transition state theory [79,80] in which tunneling effects are neglected but zero-point energies are incorporated. However, the results of the centroid simulations, which consider tunneling effects in an approximate fashion, predicts different tunneling effects for the BET2 and the BET1 or ab initio systems. In particular, it was found that r is significantly larger than the value predicted by the rule of geometric mean for the BET2 system, yielding a value of $r = 2.6 \pm 0.6$ for the

ξ_1 reaction coordinate. In addition, calculation of semi-classical transition state theory reaction rates using a harmonic description of the potential energy surface in the neighborhood of the minimum energy and transition state configurations show that the breakdown of the rule of geometric mean in the BET2 model cannot be attributed to zero point energy effects. Hence, it appears that for the proton transfer process in the BET2 system, the breakdown of the rule of geometric mean is a signature of important secondary atom tunneling effects. In contrast to the results obtained using the BET2 potential energy surface, no breakdown of the rule of geometric mean is observed for the proton transfer reaction calculations using the BET1 or the ab initio DFT potential energy surfaces (i.e. $r = 1.0$ within statistical uncertainties). Indeed, it appears that no statistically significant secondary isotope effects are evident in the BET1 and ab initio DFT systems, in accordance with chemical intuition.

The molecular mechanics potential energy surfaces BET1 and BET2 differ only in the functional form used for the variation of the bond lengths C_3O_4 and C_6O_7 (see Fig. 2 for labelling of atoms) with ξ_1 along the path of shallowest ascent. This difference translates into slight alterations in the reaction mechanism due to differing degrees of synchronization of the two most important events in the reaction, the transfer of the proton and the response of the backbone to the motion of the proton. The degree of synchronization between the motions of the transferring proton and the carbon backbone atoms can be visualized by examining the path through the configurational space of the system which contributes the most to the (quantum nuclear) free energy of the reactive process, hereafter called the *path of maximum reaction probability*. The projection of the path of maximum reaction probability on the coordinates λ and ξ_1 for the two molecular mechanics potential energy surfaces BET1 and BET2 have been extracted from the simulation results and are depicted in Fig. 3. These coordinates are convenient to analyze since the λ coordinate measures the extent of carbon backbone rearrangement while ξ_1 gauges the degree of proton displacement. The paths shown in Fig. 3 were constructed by finding the most probable value of λ for a given value of ξ_1 in the simulations after reweighting the data to compensate for the umbrella potental. These data therefore provide a clear indication of the correlation between structural rearrangements of the backbone and the motion of the proton. The results in Fig. 3 show that the proton transfer and backbone reorganization events proceed in a concerted fashion at all times for the BET1 system, whereas in the BET2 system the reaction initiates with significant proton motion, while the carbon backbone reorganizes substantially only in the transition state region.

The differing degree of carbon backbone motion in the neighborhood of the transition state observed in the simulations of the BET1 and BET2 systems is the likely cause of the difference in the magnitude of secondary atom tunneling effects. In fact, the proton transfer process in the malonaldehyde system can be effectively mapped into a simple two-dimensional model which qualitatively reproduces the heavy atom tunneling behavior as the path of maximum reaction probability changes. The projection of the path of maximum reaction probability in the parameter space spanned by λ and ξ_1 for the ab initio DFT potential reveals that the marginally significant secondary isotope effects obtained with the ab initio potential can be interpreted by means of a reaction mechanism more similar to the BET1 than to the BET2 system.

4.1 Implications and outlook

Two important theoretical questions have been addressed in the study of kinetic isotope effects in a simple model system. First, it has been demonstrated that the use of molecular mechanics potentials to study secondary kinetic isotope effects can result in artifacts unless special care is exercised in designing the molecular mechanics potential. In particular, it has been demonstrated that an unphysical molecular mechanics potential with an incorrect projection of the path of steepest descent on degrees of freedom involving secondary atom motion can result in erroneous predictions of secondary atom tunneling effects. One easy means to address this problem is to ensure that molecular mechanics potentials designed by fitting parameters from accurate electronic structure potentials correctly describe not only the energetics and structure of the minimum energy and transition state configurations, but also their eigenfrequencies and eigenmodes. In particular the projection of the eigenmode corresponding to the "imaginary frequency" at the transition state configuration on different primary and secondary atom motions should be carefully investigated.

The second theoretical question addressed concerns the partitioning of the nuclear degrees of freedom of a reactive system into quantum and classical components. Although it is generally believed that primary atoms directly involved in the bond-breaking and bond-forming processes should be treated quantum-mechanically, one might expect that treating heavy secondary atoms in a classical fashion would introduce only negligible systematic errors in the calculation of reaction rates. However this is clearly not the case when collective motions of secondary atoms play a critical role in the reaction mechanism. The BET2 system, where quantization of the nuclear degrees of freedom of the carbon atoms increased the tautomerization rate by a factor of 5, is an example of such a scenario. For systems exhibiting important heavy atom tunneling, the neglect of the quantum dispersion of the heavy nuclei can lead to errors in the calculation of rate constants of up to a factor of 10 and may well be the most significant source of systematic error in the calculation of the rate constant. Although significant secondary atom nuclear quantum effects were not observed in the model proton transfer reaction studied here when the ab initio DFT potential was used, secondary atom tunneling is likely to be important in real processes in which the reaction mechanism involves considerable motion of secondary atoms in the transition state region [81, 82]. It is therefore important to treat the quantum nuclear effects of all secondary atoms which move cooperatively as a chemical process proceeds. These conclusions, of course,

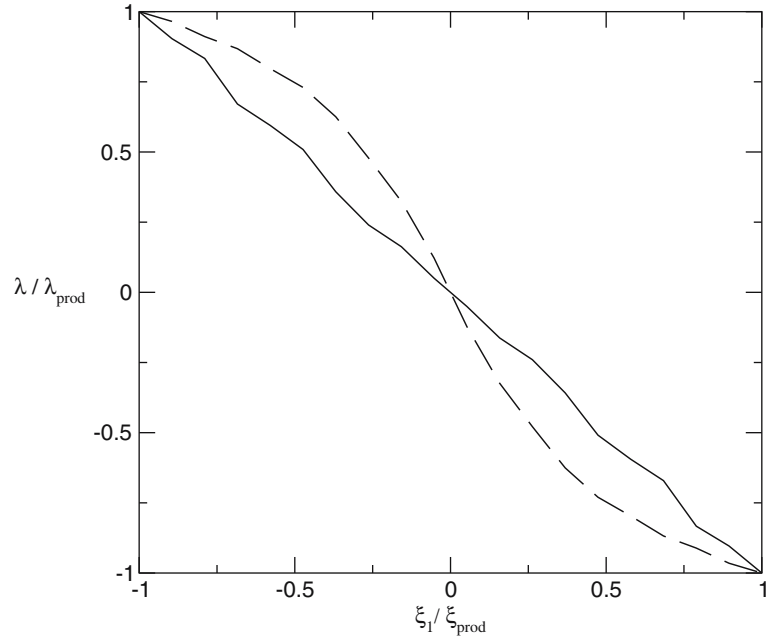

Fig. 3 A plot of the maximum density of points in the (ξ_1, λ) plane for the BET1 (*solid line*) and BET2 (*dashed line*) simulations. The maximum density of points for the ab initio simulation (not shown) follows the same profile as that of the BET1 simulation. ξ_1 is the reaction coordinate defined in Eq. (60), and $\lambda = d_{C_3O_4} - d_{C_6O_7}$ is the difference between the carbonyl and enolic bond lengths. ξ_{prod} and λ_{prod} represent the ξ_1 and λ values calculated for the product configurations

have important implications for the dynamics discussed in the Sect. 2 as well, and indicates that it is not simply the mass ratio of light and heavy nuclei that determines whether they behave classically or not.

Acknowledgements The auther would like to thank Walter Kob and the Laboratoire de Colloïdes, Verres, et Nanomatériaux in Montpellier, France for their hospitality during the period in which this manuscript was prepared.

References

1. de Groot SR, Mazur P (1962) Non-equilibrium thermodynamics, North-Holland, Amsterdam
2. Kapral R, Consta S, McWhirter L (1998) Chemical rate laws and rate constants. In: Berne BJ, Ciccotti G, Coker DF (eds) Classical and quantum dynamics in condensed phase simulations. World Scientific, Singapore, pp 583–616
3. Mori H (1965) Prog Theor Phys 33:423
4. Kapral R (1972) J Chem Phys 56:1842
5. Kubo R (1957) J Phys Soc Japan 9:570
6. Costley J, Pechukas P (1981) Chem Phys Lett 83:139
7. Yamamoto T (1960) J Chem Phys 33:281
8. Kapral R, Ciccotti G (1999) J Chem Phys 110:8919
9. Filinov VS, Bonella S, Lozovik YL, Filinov AV, Zacharov I (1998) Quantum molecular dynamics using Wigner representation. In: Berne BJ, Ciccotti G, Coker D (eds) Classical and quantum dynamics in condensed phase simulations. World Scientific, Singapore
10. Prezhdo OV, Rossky PJ (1997) J Chem Phys 107:825
11. Tully JC (1990) J Chem Phys 93:1061
12. Tully JC (1991) Int J Quantum Chem 25:299
13. Hammes-Schiffer S, Tully JC (1994) J Chem Phys 101:4657
14. McWhirter JL (1998) J Chem Phys 108:5683
15. Webster F, Rossky PJ, Friesner RA (1991) Comp Phys Comm 63:494
16. Webster FJ, Schnitker J, Friedrichs MS, Friesner RA, Rossky PJ (1991) Phys Rev Lett 66:3172
17. Coker DF, Xiao L (1995) J Chem Phys 102:496
18. Sun X, Miller WH (1997) J Chem Phys 106:916 Ibid 106:6346
19. Stock G, Thoss M (1997) Phys Rev Lett 78:578
20. Martens CC, Fang J-Y (1997) J Chem Phys 106:4918
21. Warshel A, Chu ZT (1990) J Chem Phys 93:4003
22. Miller WH (1991) J Chem Phys 95:9428
23. Heller EJ (1991) J Chem Phys 94:2723
24. Heller EJ (1991) J Chem Phys 94:9431
25. Stock G, Thoss M (1997) Phys Rev Lett 78:578
26. Herman MF, Kluk E (1984) Chem Phys 91:27
27. Kay KG (1994) J Chem Phys 100:4377–4432
28. Sun X, Wang H, Miller WH (1998) J Chem Phys 109:7064
29. Pechukas P (1969) Phys Rev 181:166
30. Tully JC, Preston RK (1971) J Chem Phys 55:562
31. Horenko I, Weiser M, Schmidt B, Schuette C (2004) J Chem Phys 120:8913
32. Truhlar DG, Gao J, Garcia-Viloca M, Alhambra C, Corchado J, Sanchez ML, Poulsen TD (2004) Int J Quantum Chem 100:1136
33. Bedard-Hearn MJ, Larsen RE, Schwartz BJ (2005) J Chem Phys 122:134506
34. Burghardt I (2005) J Chem Phys 122:094103
35. Zhu C, Jasper AW, Truhlar DG (2005) J Chem Theory Comput 1:527
36. For a more complete review of dynamics in mixed quantum – classical systems, see Sergi A, MacKernan D, Ciccotti G, Kapral R (2003) Simulating quantum dynamics in classical environments. Theor Chem Acc 110:49–58
37. Aleksandrov IV (1981) Z Naturforsch A 36a:902
38. Repts. Ukranian Acad Sci 10:65 (1981); Teor Mat Fiz 150:7 (1982)
39. Boucher W, Traschen J (1988) Phys Rev D 37:3522
40. Zhand WY, Balescu R (1988) J Plasma Phys 40:199
41. Wan C-C, Schofield J (2000) J Chem Phys 112:4447
42. Horenko I, Salzmann C, Schmidt B, Schütte C (2002) J Chem Phys 117:11075
43. Sergi A, Kapral R (2004) J Chem Phys 121:7565
44. Quinlan GD, Tremaine S (1992) Mon Not R Astron Soc 259:505

45. Toxvaerd S (1994) Phys Rev E 50:2271
46. Wan C-C, Schofield J (2000) J Chem Phys 113:7047
47. Tully JC (1990) J Chem Phys 93:1061
48. Ben-Nun M, Martínez TJ (1998) J Chem Phys 108:7244
49. Ferretti A, Granucci G, Lami A, Persico M, Villani G (1996) J Chem Phys 104:5517
50. Wan C-C, Schofield J (2002) J Chem Phys 116:494
51. Chandler D (1978) J Chem Phys 68:2959
52. Anderson JB (1995) Adv Chem Phys 91:381
53. Iverson KE (1962) A programming Language. Wiley, New York, p 11
54. Fishman GS (1996) Monte Carlo. Springer, New York
55. Topper RQ, Truhlar DG (1992) J Chem Phys 97:3647
56. Iftimie R, Schofield J (2001) J Chem Phys 115:5891
57. Iftimie R, Salahub D, Wei D, Schofield J (2000) J Chem Phys 113:4852
58. Iftimie R, Salahub D, Schofield J (2003) J Chem Phys 119:11285
59. Kohen A, Cannio R, Bartolucci S, Klinman JP (1999) Nature 399:496
60. Bahnson BJ, Colby TD, Chin JK, Goldstein BM, Klinman JP (1997) Proc Natl Acad Sci USA 94:12797
61. Cha Y, Murray CJ, Klinman JP (1989) Science 243:1325
62. Page M, Williams A (1997) Organic and bio-organic mechanisms. Addison Wesley Longman, Harlow
63. Feynman RP (1972) Statistical mechanics. Addison Wesley, Reading
64. Tuckerman ME, Berne BJ, Martyna GJ, Klein ML (1993) J Chem Phys 99:2796
65. Voth GA, Chandler D, Miller W (1989) J Chem Phys 91:7749
66. Voth GA (1993) J Phys Chem 97:8365
67. Iftimie R, Schofield J (2001) J Chem Phys 114:6763
68. Krokidis X, Goncalves V, Savin A, Silvi B (1998) J Phys Chem A 102:5065, see in particular the discussion in page 5070 and Figure 8
69. Krokidis X, Nouri S, Silvi B (1997) J Phys Chem A 101:7277
70. Pauling L (1960) The nature of chemical bond, 3rd edn. Cornell University Press, Ithaca
71. Sims LB, Lewis DE (1984) In: Buncel E, Lee CC (eds) Isotopes in organic chemistry, vol 6. Elsevier, New York
72. Warshel A, Weiss RM (1980) J Am Chem Soc 102:6218
73. Iftimie R, Schofield J (2003) Int J Quant Chem 91:404
74. Biegeleisen J (1995) J Chem Phys 23:2264
75. Ricker J, Klinman J (2001) JACS 121:1997
76. Kohen A, Cannio R, Bartolucci S, Klinman JP (1999) Nature 399:496
77. Bahnson BJ, Colby TD, Chin JK, Goldstein BM, Klinman JP (1997) Proc Natl Acad Sci USA 94:12797
78. Cha Y, Murray CJ, Klinman JP (1989) Science 243:1325
79. Saunders WH Jr (1985) J Am Chem Soc 107:164 and references therein
80. Bell RP (1973) The proton in chemistry, 2nd edn. Chapman and Hall, London
81. Lu D-h, Maurice D, Truhlar DG (1990) J Am Chem Soc 112:6206
82. Truhlar DG, Lu D-h, Tucker SC, Zhao XG, Gonzàlez-Lafont A, Truong TN, Maurice D, Liu Y-P, Lynch GC (1992) In: Kaye JA (ed) Isotope effects in chemical reactions and photodissociation processes. American Chemical Society Symposium Series 502, Washington, pp 16–36